공학석사학위논문

Structural Dynamic Analysis of Space Launch Vehicle using Axisymmetric Shell Element including Hydroelastic Effect for Pogo Stability Analysis

포고 안정성 해석을 위한 유탄성 효과가 고려된 축대칭 쉘 요소를 이용한 우주 발사체의 구조 동적 해석

2017 년 2 월

서울대학교 대학원

기계항공공학부

심 지 수

Structural Dynamic Analysis of Space Launch Vehicle using Axisymmetric Shell Element including Hydroelastic Effect for Pogo Stability Analysis

포고 안정성 해석을 위한 유탄성 효과가 고려된 축대칭 쉘 요소를 이용한 우주 발사체의 구조 동적 해석

지도교수 신 상 준

이 논문을 공학석사 학위논문으로 제출함

2017 년 2 월

서울대학교 대학원

기계항공공학부

심 지 수

심지수의 공학석사 학위논문을 인준함

2017 년 2 월

위 원 장 _____ (인)

부위원장 _____ (인)

위 원 _____ (인)

Abstract

Structural Dynamic Analysis of Space Launch Vehicle using Axisymmetric Shell Element including Hydroelastic Effect for Pogo Stability Analysis

JiSoo Sim

Department of Mechanical and Aerospace Engineering

The Graduate School

Seoul National University

Space launch vehicle exhibits many multidiscipline-related instabilities which are caused by coupling between the fuselage structural and other subsystem components. Pogo phenomenon is one of those coupled instabilities. This thesis focuses on the pogo phenomenon which is the longitudinal dynamic instability of space launch vehicles. For the prediction of the pogo phenomenon, it is essential to establish appropriate structural modeling, the characteristics of the feedlines and propulsion system. The purpose of this thesis is conducting the modal analysis of the launch vehicles. It was conducted by using the axisymmetric two-dimensional shell elements. The present analysis was validated using examples of the existing launch vehicles. The comparison in terms of modeling and results against the

existing investigations is shown. Other applications and plan for the pogo analysis are also suggested. In addition, the research about pogo phenomenon of Saturn V and space shuttle is examined in order to develop an appropriate pogo analysis using the result of the modal analysis and analyzing stability of the pogo system.

Keywords : Space launch vehicle, Pogo phenomenon, Hydroelastic effect, Stability analysis, Structural modeling, Dynamic analysis

Student Number **: 2015-20778**

Table of Contents

Abstract I

Table of Contents..... III

List of Figures..... V

List of Tables VII

List of Symbols VIII

Chapter 1. Introduction 1

1.1 Background and Motivation 4

1.2 Previous Researches 4

1.2.1 Previous Research about Pogo Phenomenon 4

1.2.2 Previous Research about Structural Modeling 5

1.3 Objectives and Thesis Overview 8

Chapter 2. Pogo Stability Analysis..... 9

2.1 Pogo Suppression on Saturn V 9

2.2 Pogo Suppression on Space Shuttle 14

Chapter 3. Structural Modeling and Modal Analysis 18

3.1 Modal Analysis of the Launch Vehicles 18

3.2 Structural Modeling of the Complete Launch Vehicle 20

3.3 Formulation 23

Chapter 4. Numerical Results and Discussion 30

4.1 Construction of the Present Analysis 30

4.2 Validation using an Example Launch Vehicle 31

Chapter 5. Conclusion and Future Works 42

5.1 Conclusion 42

5.2 Future Works 44

References 45

국문초록 52

List of Figures

Figure 1.1	Pogo phenomenon of various space launch vehicles	3
Figure 1.2	Observation of the first two Saturn V manned flight from on-board accelerometers	3
Figure 1.3	Experiment and analytical model for longitudinal dynamic test of Atlas-Centaur-Surveyor full scale model	7
Figure 2.1	Closed loop system of the pogo phenomenon	11
Figure 2.2	Simplified pogo closed loop model	12
Figure 2.3	Block diagram of simplified pogo model	13
Figure 2.4	Pogo analysis model of Space Shuttle	16
Figure 2.5	Stability result for the system without PSD when end-burn using the 34th mode	17
Figure 3.1	Structural modeling of a launch vehicle using two-dimensional shell elements	22
Figure 3.2	Displacements and the coordinate of the shell	27
Figure 3.3	Geometry of the shell component	28
Figure 3.4	Definition of fluid motion	29
Figure 4.1	Example single-stage launch vehicle	33
Figure 4.2	Relevant two-dimensional modeling	34
Figure 4.3	Numbering longitudinal direction coordinates of relevant two-dimensional modeling	36

Figure 4.4	Comparison of the 1st mode shape between the present prediction and those in Ref. 41	37
Figure 4.5	2nd and 3rd mode shapes of the present analysis	39
Figure 4.6	4th and 5th mode shapes of the present analysis	40
Figure 4.7	6th and 7th mode shapes of the present analysis	41

List of Tables

Table 4.1	Comparison of the natural frequencies between Ref. 41 and the present prediction	35
Table 4.2	Natural frequencies of example single-stage launch vehicle in the present analysis	38

List of Symbols

Symbols	Meaning
P_s	Propellant force
E	Thrust gain
f	Disturbance force
K_s	Cavitation stiffness of a pump inlet
D_s	Orifice effect of a pump
m_s	Lox mass
m	Structure mass
$[M]$	Mass matrix
$[K]$	Stiffness matrix
ω_n	Natural frequency
$[\phi]$	Mode shape vector
$u(\xi)$	Displacement of the shell component in the longitudinal direction
$\mathrm{v}(\xi)$	Displacement of the shell component in the radical direction
ξ	Dimensionless variable for the shell element
C_{11}, C_{12}, C_{22}	Orthotropic stress-strain coefficient
C_{33}, C_{34}, C_{44}	Orthotropic moment-curvature coefficient
t	Thickness of shell
γ_a	Density of the shell
γ_b	Density of the fluid

x	Coordinate in the longitudinal direction
r	Coordinate in the radial direction

Chapter 1

Introduction

1.1 Background and Motivation

Space launch vehicle has many multidiscipline-related instabilities which are especially caused by coupling between the fuselage structural and other subsystem components [1]. One of these problems are coupling between flight mechanics and bending modes of a launch vehicle. Buffet phenomenon is one between structural dynamics and aerodynamics, and longitudinal instability is a coupling between the structure and propulsion system. Such longitudinal instability is called ‘pogo’ because the motion of this phenomenon resembles the pogo stick. This thesis is primarily focused on the pogo phenomenon of a launch vehicle. The self-excited longitudinal dynamic instability arising from the interaction of the launch vehicle structure with the propulsion system. This phenomenon is one of the most complex problems in liquid propellant launch vehicles. In order to predict pogo phenomenon, its relevant analysis process requires the followings: detailed structural dynamics analysis, characteristics of feedlines, propulsion system analysis, and closed-loop feedback stability analysis. Pogo phenomenon induces damage on the payload and astronauts, in the worst case engine failure. This phenomenon occurred in many launch vehicles. Specifically, Fig. 1.1 shows the cases in launch vehicles of United

States. Most of these data are NASA human space flight program during 1960's experienced pogo phenomenon [2]. Thus, it became essential to conduct prediction of the pogo phenomenon during development of the launch vehicles. Titan II in Gemini program showed longitudinal vibration in 10-13 Hz for 30 seconds from ninety seconds after launching. This vibration became the maximum amplitude of ±2.5g about 11 Hz. Restraining it below ±0.25g was the requirements in NASA [2]. Saturn V in Apollo project also showed pogo instability. AS-502 in 1968 recorded longitudinal vibration of 5 Hz, maximum acceleration 0.6 g between 105-140 seconds during first stage(S-IC) burning. The longitudinal oscillation was observed in the first two Saturn V manned flight in Fig. 1.2. Finally, in the case of space shuttle, the passive pogo suppressor was installed to the space shuttle main engine (SSME).

Therefore, the prediction and suppression of pogo phenomenon is essentially required in the development of space launch vehicle. KSLV-II (Korea Space Launch Vehicle) which is the first launch vehicle in Korea responsible for complete system is being developed. Under that circumstances, the fundamental research of the pogo phenomenon is expected to be one of the important contributions in the future space launch vehicle development.

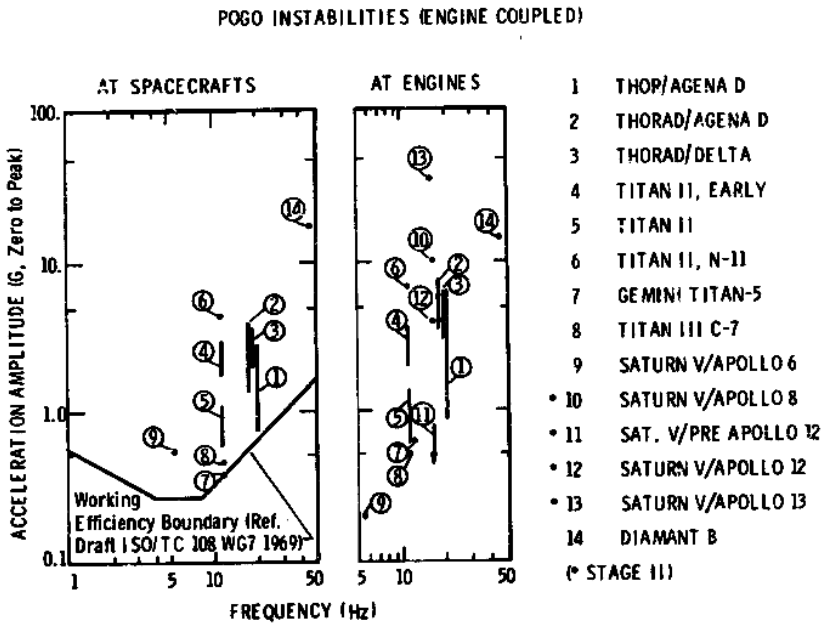

Figure 1.1 Pogo phenomenon of various space launch vehicles [3]

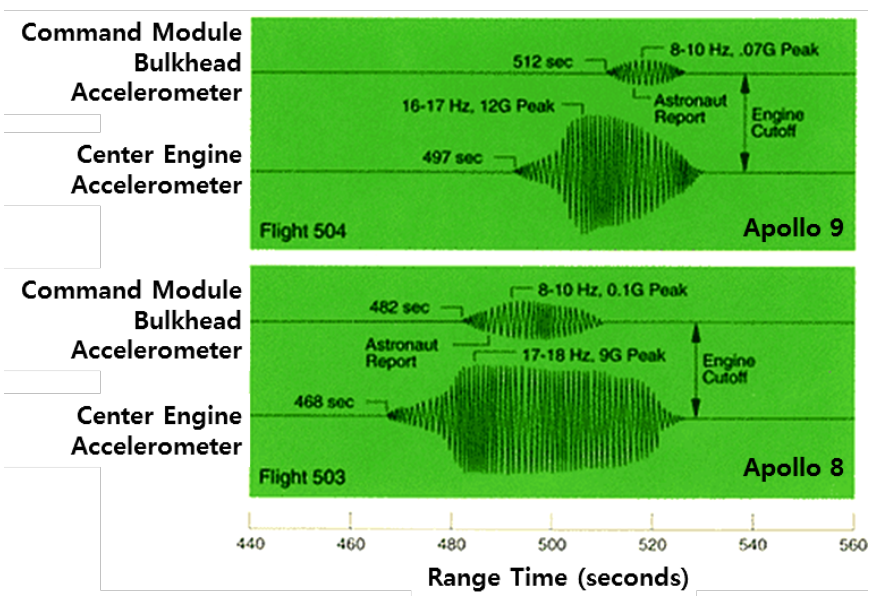

Figure 1.2 Observation of the first two Saturn V manned flight from on-board accelerometers [4]

1.2 Previous Research

1.2.1 Previous Research about Pogo Phenomenon

As mentioned in the previous section, accurate prediction capability of the pogo phenomenon is required critically. A few researchers have conducted research about the pogo phenomenon since 1960's. Rubin[5] and Oppenheim[6] developed stability analysis of the pogo phenomenon. A launch vehicle, feedlines, and propulsion system were substituted with their mathematical models. Those models were linear time invariant systems. The system of the pogo phenomenon was composed of the closed-loop system. The possibility of the pogo phenomenon was decided by examining stability of that system. For accurate closed-loop pogo stability analysis, it is substantially required to predict accurate natural vibration characteristics of the vehicle structures and feedlines.

While looking for specific research about pogo phenomenon depending on launch vehicles, many of those, such as Delta[7], Atlas[6], Titan[8, 9], Saturn V[10-13], and space shuttle[14-20] were analyzed in USA. Accumulator for Ares I-X was considered[21]. Passive pogo suppression device was applied to these launch vehicles. There is NASA space vehicle design criteria document for pogo[22]. The Ariane series in Europe and H-II in Japan were also used for the research about pogo[23-28]. Chinese researchers studied pogo phenomenon recently. Zhao at el[29] conducted the relevant parametric study. Xu at el[30] and Hao at el[31] developed the method using NASTRAN for the structural system,

rational function method, and finite element method for the propulsion system. In Korea, research was conducted about KSR-III[32, 33].

1.2.2 Previous Research about Structural Modeling

In order to predict pogo phenomenon, structural dynamic characteristics of the launch vehicle is essential. Therefore, this thesis is concentrated on the structural analysis of a launch vehicle in order for stability analysis of the pogo phenomenon. There exist a lot of research for the modal analysis and experiments of the launch vehicles. Structural modeling is proceeded for structural analysis. For efficient modeling, one-dimensional modeling was developed since 1960s-70s. One–dimensional modeling is conducted using the lumped masses and one-dimensional springs. Such methodology was published in many NASA documents[34-38] and criteria[39, 40]. Especially, that attempt of the one-dimensional modeling focused on interaction between the tanks and liquid propellants, called the hydroelastic effect. Because the characteristics of the tank component were significantly influential upon the launch vehicle, such hydroelastic effect was needed to be reflected in the one-dimensional modeling. The example of one-dimensional modeling is shown in Fig. 1.3.

Two- and three-dimensional modeling were considered for more accurate analysis. Archer et al[41, 42] developed the method and program for structural modeling using two-dimensional axisymmetric shell. Furthermore, Saturn V[43] and space shuttle[44] were modeled using NASTRAN earlier. Comparisons on the

natural frequencies and mode shapes between the analyses and experiments were attempted. As one of those attempts, Kim developed a method of the one-dimensional modeling for the space launch vehicle [45, 46].

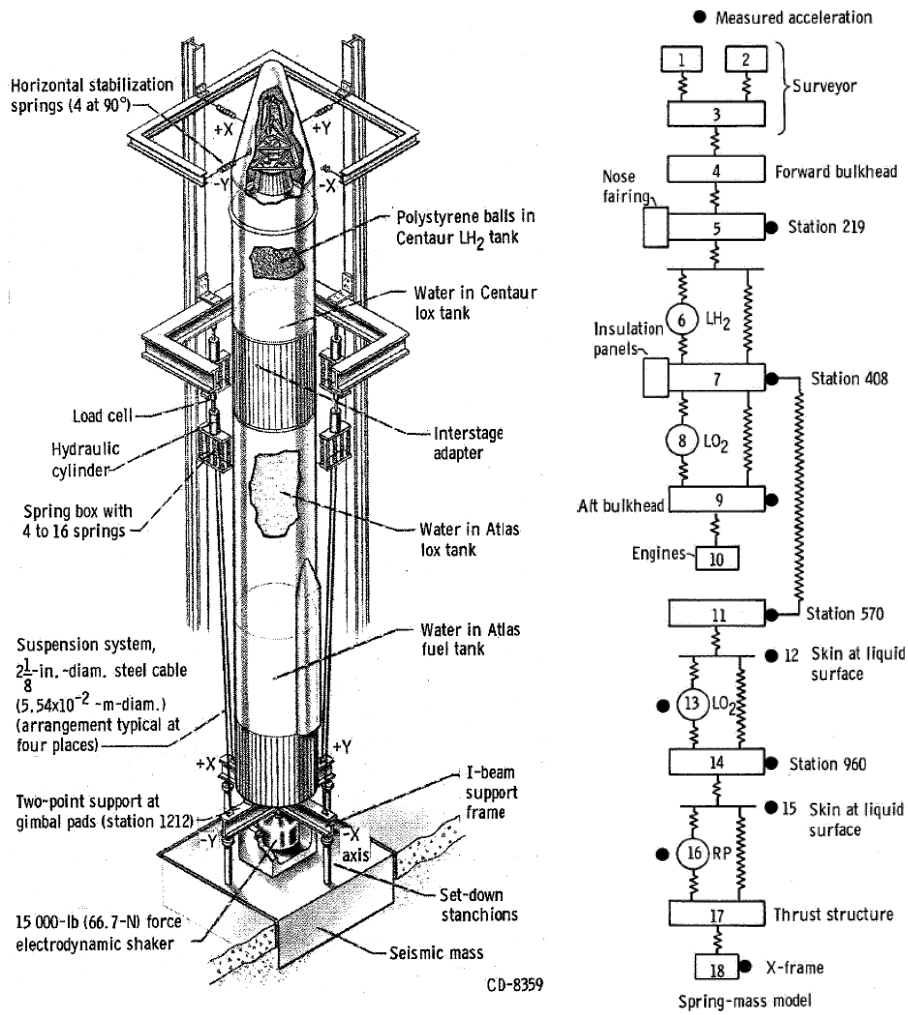

(a) Longitudinal dynamic test **(b) Mass- spring model**

Figure 1.3 Experimental and analytical model for longitudinal dynamic test of Atlas-Centaur-Surveyor full scale model [47]

1.3 Objectives and Thesis Overview

This thesis will examine complete process for predicting the pogo phenomenon. In many documents and articles which were have been developed since 1960s, the fundamental research about pogo phenomenon was developed. Especially, pogo stability analysis and structural modeling is focused in order to predict pogo phenomenon.

For these purpose, it is essential that modal analysis of a complete space launch vehicle will need to be conducted. In order for the modal analysis, structural modeling will be required and developed. Two-dimensional modeling is considered to upgrade the previous one-dimensional modeling in order for more accurate and straightforward analysis[48]. In more detail, this thesis adopts two-dimensional axisymmetric shell element for structural modeling. Consideration of the hydroelastic effect will be critically important in this method. A relevant in-house program will be constructed in MATLAB. Such program will be validated using an example launch vehicle. As a result, modal analysis will be conducted using this methodology. Structural dynamic characteristics will be obtained through the modal analysis of a space launch vehicle.

In addition to focusing on the structural dynamic analysis, the research about pogo stability analysis will also be conducted. Because many documents of Saturn V and space shuttle about the pogo phenomenon exist, research will be conducted and its results will be included in this. The final goal of this thesis is to conduct pogo stability analysis using the result of the modal analysis.

Chapter 2

Pogo Stability analysis

2.1 Pogo Suppression on Saturn V

In Chapter 2, analysis of the pogo phenomenon is examined and developed on the examples of Saturn V and space shuttle. Fundamentally, pogo phenomenon is analyzed by two transfer functions of the closed loop system. The first is related with the structural system, $G(s)$, and the other is related with the propulsion system, $H(s)$, as shown in Fig. 2.1. Therefore, it is required that *G(s)* and *H(s)* should reflect the characteristics of the realistic system accurately. This closed system will be analyzed regarding the certain condition which is a possibility for the pogo phenomenon. Finally, the pogo phenomenon will be predicted by dependence on the stability of this closed system.

Pogo stability investigation of Saturn V was conducted by Sterett et al[49]. He provided a complete summary about evolution of the pogo analysis methodology. He also analyzed the second stage, S-II, and the third stage, S-IVB as well as the first stage, S-IC. von Pragenau[11] suggested a simplified pogo closed loop model, as shown in Fig. 2.2. In his result, the relation among the propellant force P_s, thrust T, the force F_s, and disturbance force f was obtained as written in Eqs. (1), (2).

$$P_s \cdot E = T \tag{1}$$

$$F_s = P_s \cdot E + f \tag{2}$$

The relevant expression among the system, the propellant force, and the force is also given in Eq. (3)

$$P_s = \frac{F_s}{1 + \frac{m}{m_s} + s\frac{m}{D_s} + s^2\frac{m}{K_s}} \tag{3}$$

The closed loop equation will become complete by combining Eqs. (2) and (3). Then, the resulting equation will be as follows.

$$P_s = \frac{f}{1 + \frac{m}{m_s} - E + s\frac{m}{D_s} + s^2\frac{m}{K_s}} \tag{4}$$

Finally, the stability will be determined by the sign of the eigenvalues *s*. Such determination criterion is expressed in Eq. (5).

$$E < 1 + \frac{m}{m_s} \tag{5}$$

This complete relation of the closed-loop system is illustrated by the block diagram shown in Fig. 2.3. This result is one simplified example of the process of analyzing pogo phenomenon.

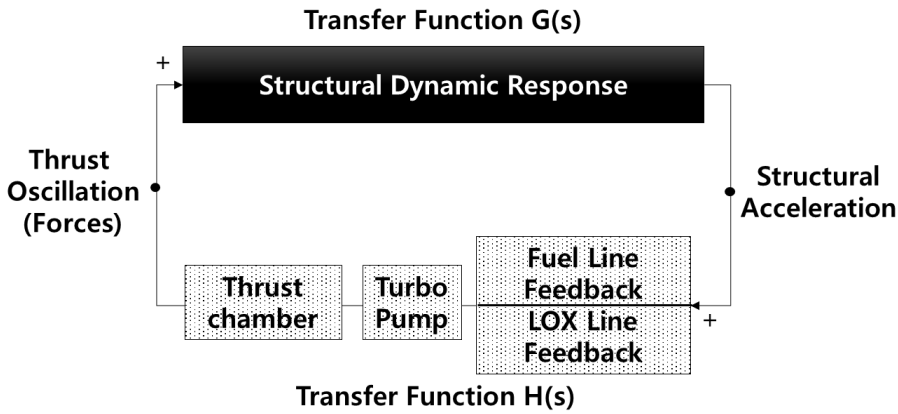

Figure 2.1 Closed loop system of the pogo phenomenon

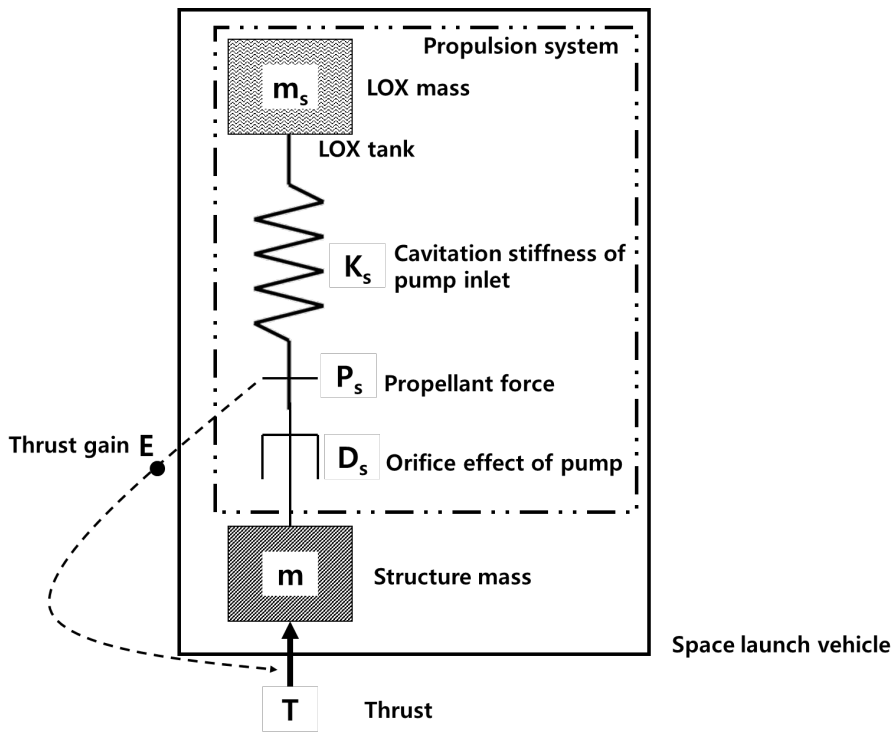

Figure 2.2 Simplified pogo closed loop model

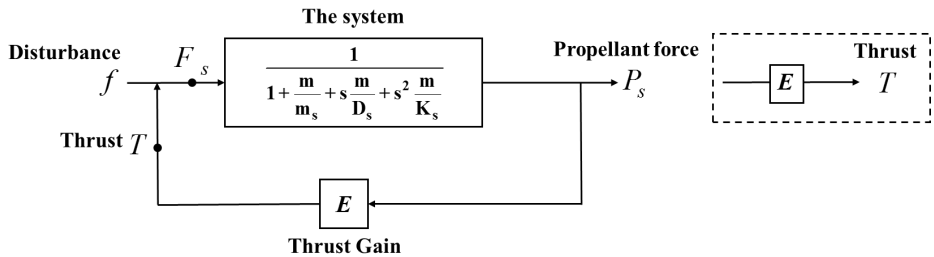

Figure 2.3 Block diagram of a simplified pogo analysis

2.2 Pogo Suppression in Space Shuttle

In the case of the space shuttle, relevant pogo integration panel was organized for discussing and deciding the methodology of the pogo suppression in the space shuttle by various NASA research centers and contractors[14]. As a result, passive pogo suppression device was installed even though both passive and active devices were suggested simultaneously. The analytical model and the method was noticeable. Because of the specific configuration of the space shuttle having an external tank, a feedline of significant length (31 m) was utilized. Liquid oxygen is quite heavier than liquid hydrogen, which was the main fuel of the space shuttle. Therefore, the analytical model of the space shuttle for predicting pogo was composed of only LOX tank, longitudinal lateral feedline, low and high LOX pump, and chamber[16, 17], as shown in Fig 2.4. A few specific flight conditions, lift off, max. *Q*, before solid rocket booster (SRB) jettison, after SRB jettison, which have high possibility for pogo instability were selected and analyzed. The analytical model used was composed of 14 variables which were the generalized coordinates for the structural system, pressures, and the flow rates for propulsion system, as listed in Eq. (6).

$$\hat{H} = \{P_2, P_4, P_5, P_7, P_8, P_c, Q_t, Q_2, Q_3, Q_4, Q_5, Q_7, Q_8, q_n\} \tag{6}$$

$$\{[V(s)] + [E][F(s)]\} \cdot \hat{H} = 0 \tag{7}$$

The complete system became the 14th order system, as written in Eq. (7). [*V(s)*] is the complete system composed of both structural and propulsion system. [*E*] is the

position of the pogo suppression device. [*F(s)*] is the characteristic of the pogo suppression device. Pogo instability was determined through an eigenvalue analysis of the system by employing several structural modes of each flight condition and varying the natural frequencies of ±15%. The result of the analysis is shown in Fig. 2.5. This case was the end-burn using the 35^{th} mode. The pogo instability occurred when the damping ratio decreased quite significantly and became negative. Such process of analysis suggested what would be required for constructing the pogo analysis. The first would be the characteristics of the structural system in terms of the general coordinates, q. And the second would be the mathematical model of the feedlines and propulsion system in terms of the pressures and flow rates. The relation of the structural system, q and propulsion system, P and Q would be essentially needed.

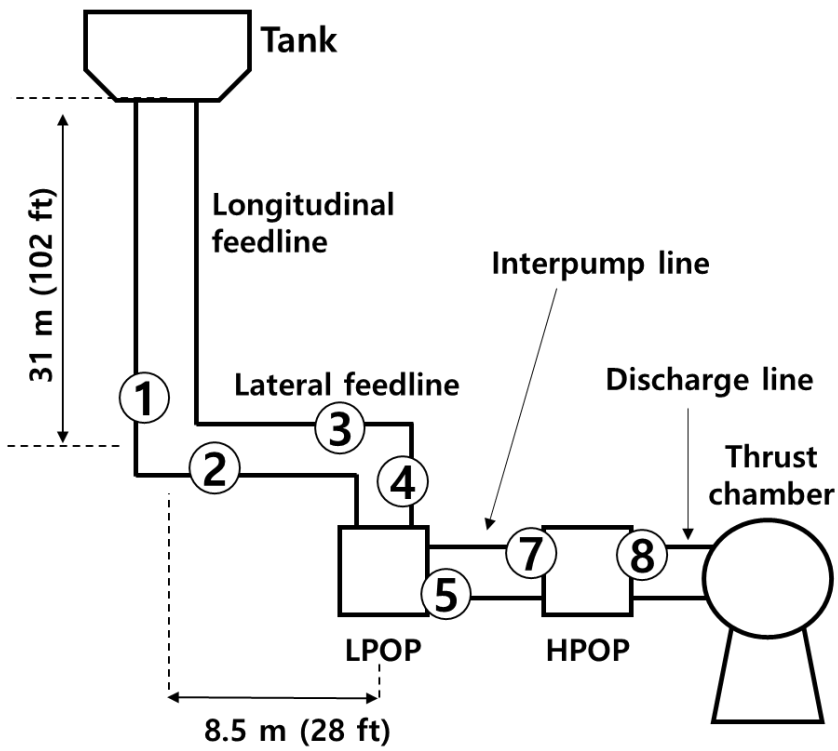

Figure 2.4 Pogo analysis for the space shuttle

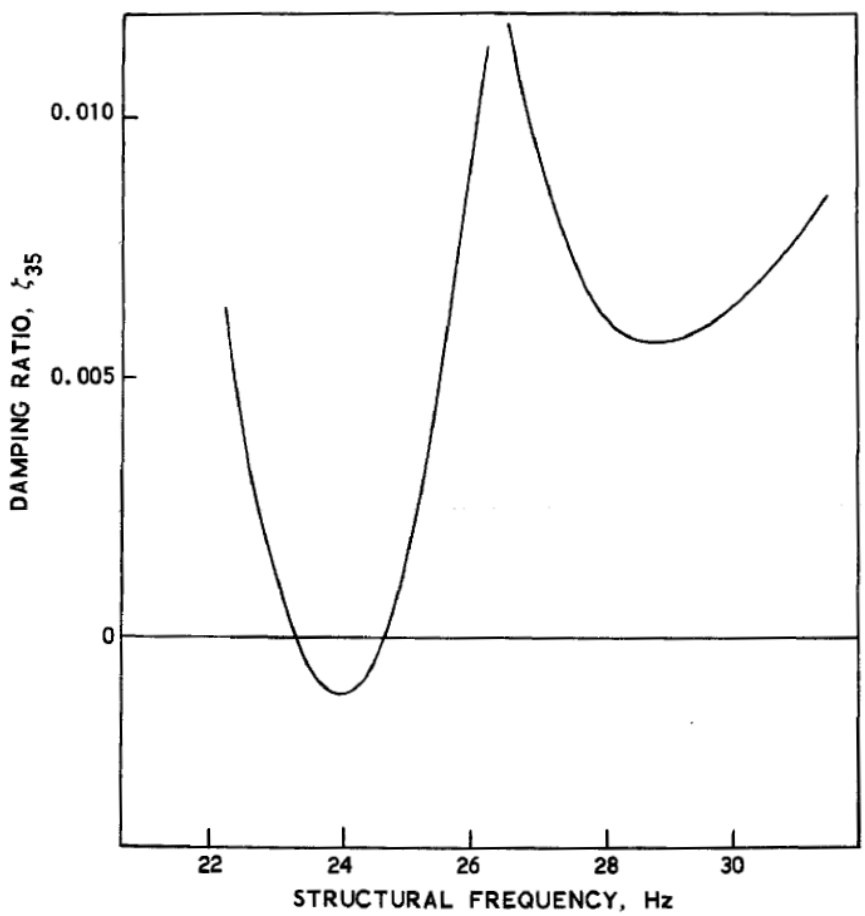

Figure 2.5 Stability result of the space shuttle

without the suppressor for the end-burn using the 34th mode [16]

Chapter 3

Structural Modeling and Modal Analysis

3.1 Modal Analysis of the Launch Vehicles

This thesis focuses on the structural dynamic response of a launch vehicle. For predicting the response, transfer function *G(s)* in Fig. 2.1 will be required. Transfer function *G(s)* is the natural frequencies and mode shapes of the launch vehicle. Modal analysis needs to be conducted for obtaining the transfer function *G(s)* via an appropriate structural modeling. Modal analysis can be expressed in the equations as follows. Assuming a launch vehicle to be an undamped system, mass and stiffness matrices are used in the modal analysis, as written in Eq. (8).

$$[M]\{\ddot{x}\}+[K]\{x\}=0 \tag{8}$$

$$\omega_n^2[M]\{x\}+[K]\{x\}=0 \tag{9}$$

$$\omega_n^2\{x\}=-[K][\mathrm{M}]^{-1}\{x\} \tag{10}$$

Equation (8) can be rearranged to become Eq. (10). Equation (10) is an eigenvalue problem statement. When the eigenvalue problem is analyzed,

eigenvalues will become the natural frequencies and eigenvectors become the mode shapes. Equation (11) is a generalized form using the natural frequencies and mode shapes. Equation (11) shows the situation when the resultant force (excitation) exits. It is expressed in terms of the generalized coordinates; *{ξ}* is the modal displacements.

$$[M][\phi]\{\ddot{\xi}\}+[\mathrm{K}][\phi]\{\xi\}=0 \tag{11}$$

$$\{\ddot{\xi}\}+[\Omega]\{\xi\}=0 \tag{12}$$

$$\{\ddot{\xi}\}+[\Omega]\{\xi\}=[\phi]^{T}[F] \tag{13}$$

When Eqs. (12) and (13) are obtained, transfer function *G(s)* will be constructed.

3.2 Structural Modeling of the Complete Launch Vehicle

Structural modeling is the first step for the modal analysis. Structural modeling is obtaining the mass and stiffness matrices of a launch vehicle. The method of the structural modeling is categorized by the dimension of the elements used. In this thesis, two-dimensional shell element is used for the structural modeling. This element is concretely two-dimensional axisymmetric shell element. Archer and Rubin[41] suggested this methodology and the relevant program was developed using this method. The purpose of the program was to predict the structural dynamics of axisymmetric launch vehicle focused on the longitudinal direction. This thesis also uses such method and explains the method as follows.

Liquid launch vehicle is composed of the payload, tank, propellant, engine, instruments, and external shells. The characteristics of each component are considered for the structural modeling. This method disassembles a launch vehicle into three components; spring-mass component, shell component, and fluid component. Spring-mass component means lumped mass and one direction massless spring. This element is the same one used in the previous one-dimensional structural modeling method. Payload, engine, and instruments are modelled by the spring-mass components that are heavy weight and exhibit little influence upon the structure. Tanks and external shells are modelled by using the shell components. This component is used in the most part of the launch vehicle. This element contributes to the creation of the mass and stiffness matrices. The

detailed mathematical process uses Rayleigh-Ritz method. The shell element has longitudinal, radial, rotational coordinates. Then, the shell elements are divided into upper elliptical bulkhead, lower elliptical bulkhead, and conical shell according to geometry of the shell. Fluid component is used to represent the liquid propellant. The fluid component has the same coordinate as the shell element does, but creates only mass matrix. Fluid component is surrounded with three shell elements; upper bulkhead, conical shell, lower bulkhead. This element does not create additional degree of freedom as the virtual mass in NASTRAN does. The complete process is shown in Fig. 3.1.

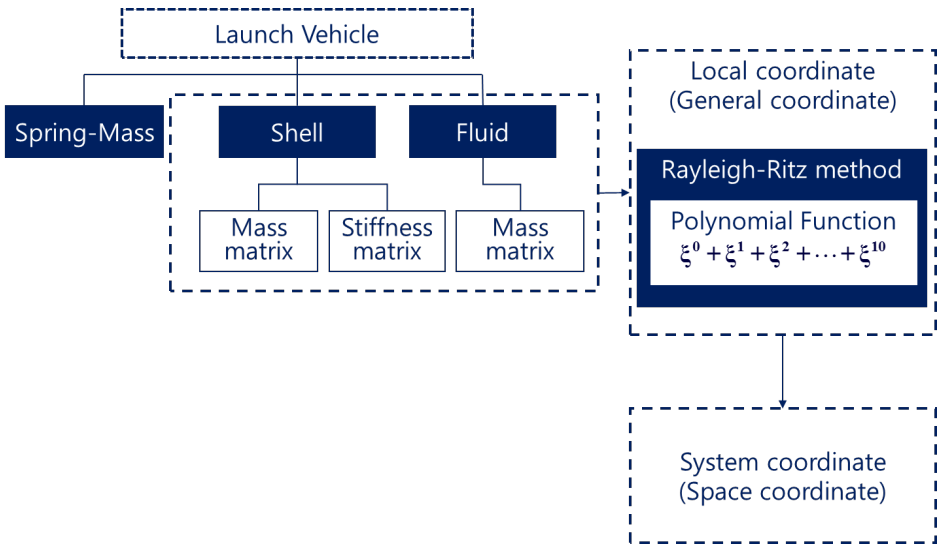

Figure 3.1 Structural modeling of a launch vehicle

using two-dimensional shell elements

3.3 Formulation

The implementation procedure of the formulation for the shell element is performed by using Rayleigh-Ritz method based on the polynomial function. The displacement of an individual shell component is expressed in Eqs. (14) and (15).

$$u(\xi)=\sum_{k=1}^{\bar{U}}\bar{\alpha}_k u_k(\xi) \tag{14}$$

$$v(\xi)=\sum_{l=1}^{\bar{V}}\bar{\beta}_l v_l(\xi) \tag{15}$$

$$u_2(\xi)=1+\xi^2 \quad , \quad v_2(\xi)=\xi^1+\xi^2 \tag{16}$$

Displacements of the shell and the direction of *u(ξ), v(ξ)* coordinates are shown in Fig. 3.2. Equation (16) is an example of the mode shape using the polynomial function. ξ is a dimensionless variable according to the geometry of the shell. This variable can be described under the following three categories; conical shell, upper bulkhead, and lower bulkhead, as shown in Fig. 3.3.

$$\xi=\frac{s}{\ell}\sin\phi_o \tag{17}$$

$$\xi=\frac{\phi}{\phi_o} \tag{18}$$

$$\xi = \frac{\pi - \phi}{\pi - \phi_o} \tag{19}$$

Equations (17), (18), and (19) are the dimensionless variables of the conical shell, upper bulkhead, lower bulkhead. The shell stiffness and mass matrix are shown in Eqs. (20), (21).

$$[K] = \begin{bmatrix} \frac{\partial^2 V}{\partial \bar{\alpha}_1 \partial \bar{\alpha}_1} \cdots \frac{\partial^2 V}{\partial \bar{\alpha}_1 \partial \bar{\alpha}_{\bar{U}}} & \frac{\partial^2 V}{\partial \bar{\alpha}_1 \partial \bar{\beta}_1} \cdots \frac{\partial^2 V}{\partial \bar{\alpha}_1 \partial \bar{\beta}_{\bar{V}}} \\ \vdots \quad \vdots & \vdots \quad \vdots \\ \frac{\partial^2 V}{\partial \bar{\alpha}_{\bar{U}} \partial \bar{\alpha}_1} \cdots \frac{\partial^2 V}{\partial \bar{\alpha}_{\bar{U}} \partial \bar{\alpha}_{\bar{U}}} & \frac{\partial^2 V}{\partial \bar{\alpha}_{\bar{U}} \partial \bar{\beta}_1} \cdots \frac{\partial^2 V}{\partial \bar{\alpha}_{\bar{U}} \partial \bar{\beta}_{\bar{V}}} \\ \frac{\partial^2 V}{\partial \bar{\beta}_1 \partial \bar{\alpha}_1} \cdots \frac{\partial^2 V}{\partial \bar{\beta}_1 \partial \bar{\alpha}_{\bar{U}}} & \frac{\partial^2 V}{\partial \bar{\beta}_1 \partial \bar{\beta}_1} \cdots \frac{\partial^2 V}{\partial \bar{\beta}_1 \partial \bar{\beta}_{\bar{V}}} \\ \vdots \quad \vdots & \vdots \quad \vdots \\ \frac{\partial^2 V}{\partial \bar{\beta}_{\bar{V}} \partial \bar{\alpha}_1} \cdots \frac{\partial^2 V}{\partial \bar{\beta}_{\bar{V}} \partial \bar{\alpha}_{\bar{U}}} & \frac{\partial^2 V}{\partial \bar{\beta}_{\bar{V}} \partial \bar{\beta}_1} \cdots \frac{\partial^2 V}{\partial \bar{\beta}_{\bar{V}} \partial \bar{\beta}_{\bar{V}}} \end{bmatrix} \tag{20}$$

$$[\mathrm{M}] = \begin{bmatrix} \frac{\partial^2 T}{\partial \bar{\alpha}_1 \partial \bar{\alpha}_1} \cdots \frac{\partial^2 T}{\partial \bar{\alpha}_1 \partial \bar{\alpha}_{\bar{U}}} & \frac{\partial^2 V}{\partial \bar{\alpha}_1 \partial \bar{\beta}_1} \cdots \frac{\partial^2 V}{\partial \bar{\alpha}_1 \partial \bar{\beta}_{\bar{V}}} \\ \vdots \quad \vdots & \vdots \quad \vdots \\ \frac{\partial^2 T}{\partial \bar{\alpha}_{\bar{U}} \partial \bar{\alpha}_1} \cdots \frac{\partial^2 T}{\partial \bar{\alpha}_{\bar{U}} \partial \bar{\alpha}_{\bar{U}}} & \frac{\partial^2 V}{\partial \bar{\alpha}_{\bar{U}} \partial \bar{\beta}_1} \cdots \frac{\partial^2 V}{\partial \bar{\alpha}_{\bar{U}} \partial \bar{\beta}_{\bar{V}}} \\ \frac{\partial^2 V}{\partial \bar{\beta}_1 \partial \bar{\alpha}_1} \cdots \frac{\partial^2 V}{\partial \bar{\beta}_1 \partial \bar{\alpha}_{\bar{U}}} & \frac{\partial^2 T}{\partial \bar{\beta}_1 \partial \bar{\beta}_1} \cdots \frac{\partial^2 T}{\partial \bar{\beta}_1 \partial \bar{\beta}_{\bar{V}}} \\ \vdots \quad \vdots & \vdots \quad \vdots \\ \frac{\partial^2 V}{\partial \bar{\beta}_{\bar{V}} \partial \bar{\alpha}_1} \cdots \frac{\partial^2 V}{\partial \bar{\beta}_{\bar{V}} \partial \bar{\alpha}_{\bar{U}}} & \frac{\partial^2 T}{\partial \bar{\beta}_{\bar{V}} \partial \bar{\beta}_1} \cdots \frac{\partial^2 T}{\partial \bar{\beta}_{\bar{V}} \partial \bar{\beta}_{\bar{V}}} \end{bmatrix} \tag{21}$$

V and T are the potential and kinetic energy, respectively. The coordinate used in the modeling of the shell component is shown in Fig. 3.3.

$$V = \frac{1}{2}\int_s 2\pi r\left(N_\phi\, \varepsilon_\phi + N_\theta\, \varepsilon_\theta + M_\phi\, K_\phi + M_\phi\, K_\phi + N_\phi{}^o\, \rho^2 \right) ds \tag{22}$$

$$\frac{\partial^2 V}{\partial \bar{\alpha}_k\, \partial \bar{\beta}_l} = 2\pi \int_s r \left\{ \begin{aligned} &\left[\mathrm{C}_{11} \frac{\partial \varepsilon_\phi}{\partial \bar{\alpha}_k} + \mathrm{C}_{12} \frac{\partial \varepsilon_\theta}{\partial \bar{\alpha}_k} \right] \frac{\partial \varepsilon_\phi}{\partial \bar{\beta}_l} \\ &\quad + \left[\mathrm{C}_{12} \frac{\partial \varepsilon_\phi}{\partial \bar{\alpha}_k} + \mathrm{C}_{22} \frac{\partial \varepsilon_\theta}{\partial \bar{\alpha}_k} \right] \frac{\partial \varepsilon_\theta}{\partial \bar{\beta}_l} \\ &\quad + \left[\mathrm{C}_{33} \frac{\partial K_\phi}{\partial \bar{\alpha}_k} + \mathrm{C}_{34} \frac{\partial K_\theta}{\partial \bar{\alpha}_k} \right] \frac{\partial K_\phi}{\partial \bar{\beta}_l} \\ &\quad + \left[\mathrm{C}_{34} \frac{\partial K_\phi}{\partial \bar{\alpha}_k} + \mathrm{C}_{44} \frac{\partial K_\theta}{\partial \bar{\alpha}_k} \right] \frac{\partial K_\theta}{\partial \bar{\beta}_l} \\ &\quad + N_\phi^o \frac{\partial \rho}{\partial \bar{\alpha}_k} \frac{\partial \rho}{\partial \bar{\beta}_l} \end{aligned} \right\} ds \tag{23}$$

Each elemental stiffness matrix is formulated in Eq. (23); potential energy is in Eq. (22). C_{11}, C_{12}, C_{22}, C_{33}, C_{34}, C_{44} are the orthotropic stress-strain and orthotropic moment-curvature coefficients. Finally, the elemental stiffness and mass matrix are obtained as in Eqs. (24) and (25). K_1, K_2, ... , *and* K_{13} are the approximate analytical coefficients.

$$[K] = 2\pi \int r \left(\begin{aligned} &\int r\,(K_1 \cdot \{\dot{\mathrm{u}}\} \cdot \{\dot{\mathrm{u}}\}^T + K_2 \cdot \{\ddot{\mathrm{u}}\} \cdot \{\ddot{\mathrm{u}}\}^T \\ &\qquad + K_3 \cdot [\{\dot{\mathrm{u}}\} \cdot \{\ddot{\mathrm{u}}\}^T + \{\ddot{\mathrm{u}}\} \cdot \{\dot{\mathrm{u}}\}^T] \\ &\qquad + K_4 \cdot [\{\mathrm{v}\} \cdot \{\dot{\mathrm{v}}\}^T + \{\dot{\mathrm{v}}\} \cdot \{\mathrm{v}\}^T] \\ &\qquad + \cdots + K_{13} \cdot [\{\ddot{\mathrm{v}}\} \cdot \{\ddot{\mathrm{u}}\}^T + \{\ddot{\mathrm{u}}\} \cdot \{\ddot{\mathrm{v}}\}^T] \end{aligned} \right) r_1\, d\phi \tag{24}$$

$$[M] = 2\pi t \int r \left(\{\mathrm{u}\} \cdot \{\mathrm{u}\}^T + \{\mathrm{v}\} \cdot \{\mathrm{v}\}^T \right) \mathrm{ds} \tag{25}$$

Fluid component provides only the mass matrix. The fluid motion is expressed

in terms of a function of the generalized displacements for the shell components. The fluid motion and coordinate are shown in Fig. 3.4. Mass matrix of the fluid component is obtained by Eq. (26). This fluid is assumed to be incompressible and inviscid. $\hat{u}_m(x)$ is equal to the change in volume below a given location x divided by the corresponding tank cross sectional area. Radial fluid motion varies linearly with the space coordinate.

$$[M] = 2\pi\gamma_b \int_{-\bar{H}_3}^{H} \int_0^r \left(\{\hat{u}(x)\} \cdot \{\hat{u}(x)\}^T + \{\hat{v}(x,\hat{r})\} \cdot \{\hat{v}(x,\hat{r})\}^T \right) d\hat{r}\, dx \tag{26}$$

Each component of the shell and fluid is estimated to provide the mass and stiffness matrices. These matrices are in the local coordinate (generalized coordinate) shown in Fig. 3.1. These matrices can be transformed into the system coordinate (space coordinate). As a result, all the components are combined to give one mass and one stiffness matrix of the system. This completes the structural modeling.

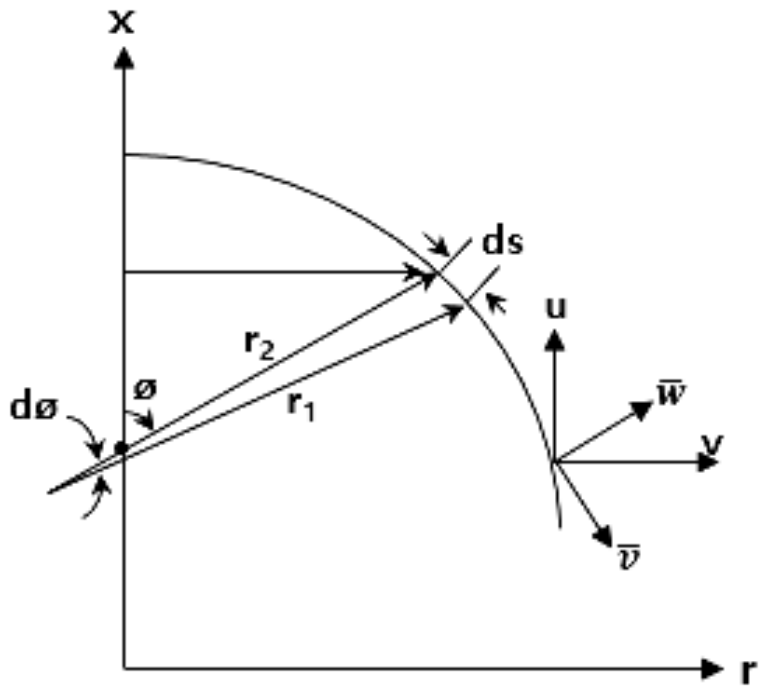

Figure 3.2 Displacements and the coordinate of the shell

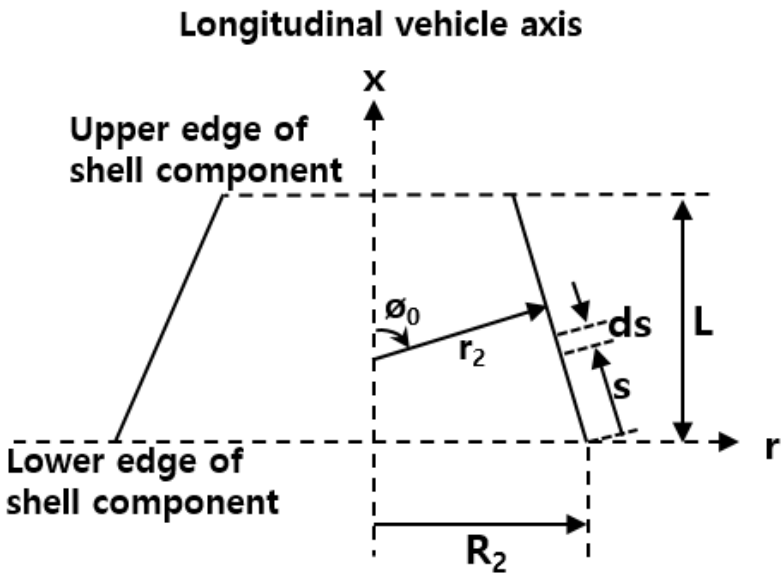

(a) conical shell

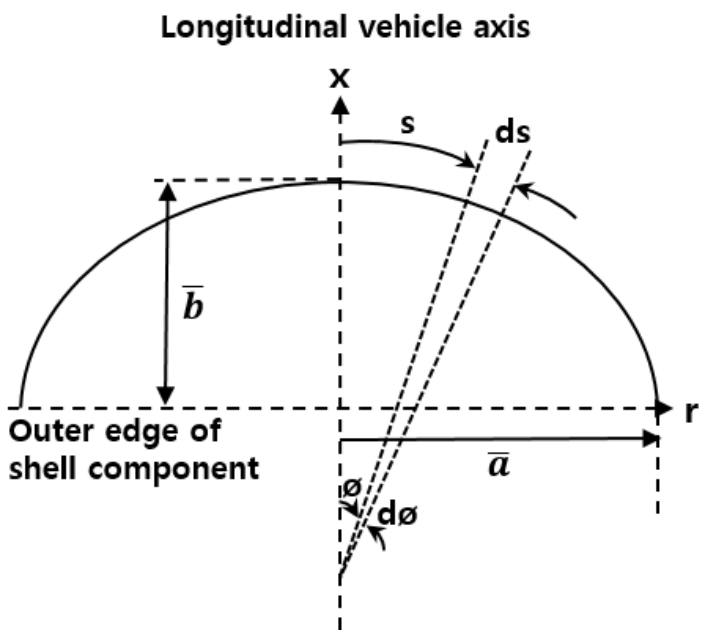

(b) elliptical bulkhead

Figure 3.3 Geometry of the shell component

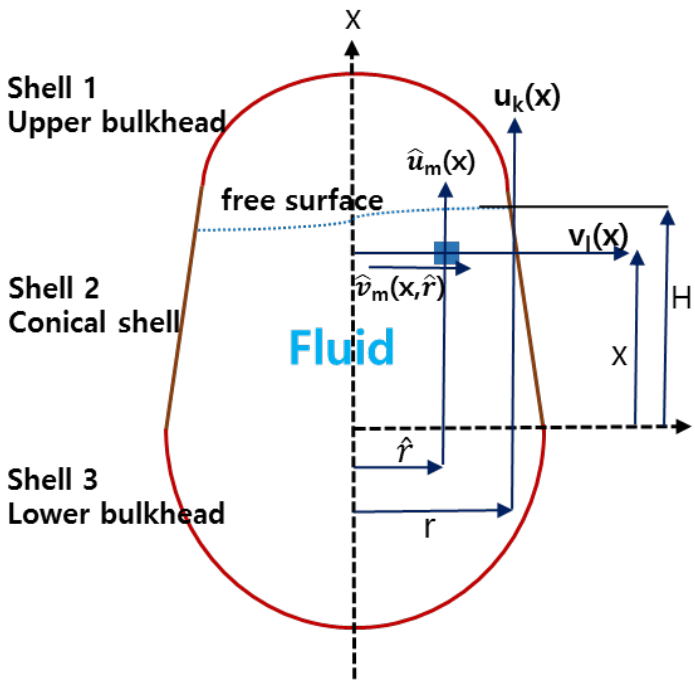

Figure 3.4 Definition of fluid motion

Chapter 4

Numerical Results and Discussion

4.1 Construction of In-house Program

The present in-house program is developed using the methodology explained in the previous chapters. MATLAB is used for the baseline program. The variable ‘sym’ is used to represent the symbolic variables for the normalized variable changing from 0 to 1. The function ‘int’ is used to express the definite integral for the matrix element. Eigenvalue problem is solved by the function ‘eig’. The present numerical integration was conducted using a variable size of steps in MATLAB for more accuracy instead of 16-point Gaussian weighting methodology in Ref. 41.

4.2 Validation using an Example Launch Vehicle

Example input and output is provided in Refs. 41 and 42(Figs. 4.1 and 4.2). The present example is the single-stage liquid launch vehicle that is axisymmetric as shown in Fig. 4.1. The further structural modeling of that example is shown in Fig. 4.2. Its modeling is composed of 11 shell components, 4 spring mass components, and 2 fluid components and has total 30 degrees of freedom. Four spring-mass elements are used to represent the payload, equipment, and engine. Two fluid components are used to represent the oxidizer and fuel. Using these data, the present program is to be validated. Mass and stiffness matrices are compared for each element against those in Ref. 41. The difference for each element is smaller than 2%. Finally, mass and stiffness matrices of 30×30, are obtained for the present example launch vehicle. Eigenvalue problem is solved by using these matrices. Natural frequencies are then obtained by the present program. Table 4.1 shows the comparison of the natural frequencies against those in Ref. 41. The two sets of the results show good agreement.

Comparison of the first mode shape between the present prediction and those in Ref. 41 is shown in Fig. 4.4. The relevant two-dimensional modeling uses 30 coordinates, as shown in Fig. 4.3. These coordinates are composed of ones in the longitudinal, radial, and rotational directions. Among those, only the longitudinal direction coordinates are used to show the relevant mode shapes, as in Fig. 4.3. In Fig. 4.4, the blue line designates the mode shape of the complete launch vehicle in the longitudinal direction. The black squares are the coordinates of the tanks. It is

possible to be the outside of the blue line because the bulkheads exist inside of the launch vehicle. Both mode shapes are in good agreement. This shows that the present in-house analysis correlates well in terms of the natural frequencies and mode shapes. All natural frequencies except the rigid body mode are shown in Table 4.2 which is the result of the present analysis. The other mode shapes of the example single-stage launch vehicle in the present analysis are shown in Figs. 4.5, 4.6, and 4.7, respectively.

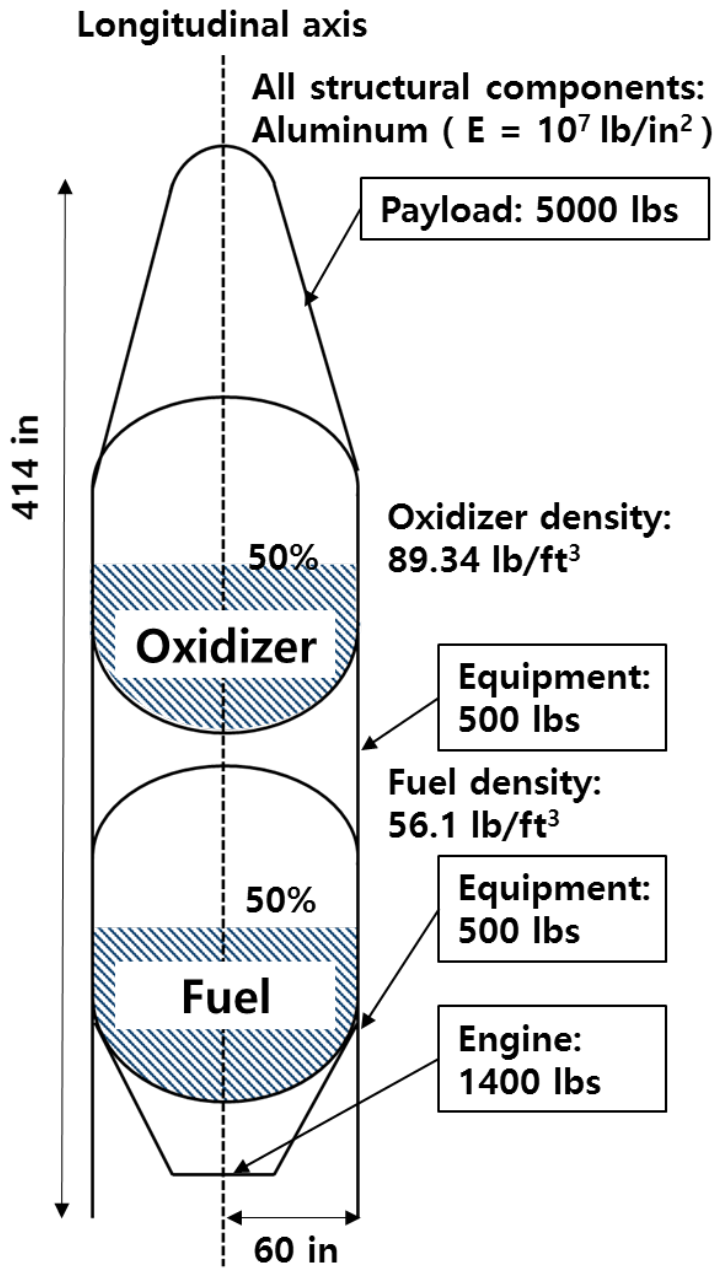

Figure 4.1 Example single-stage launch vehicle

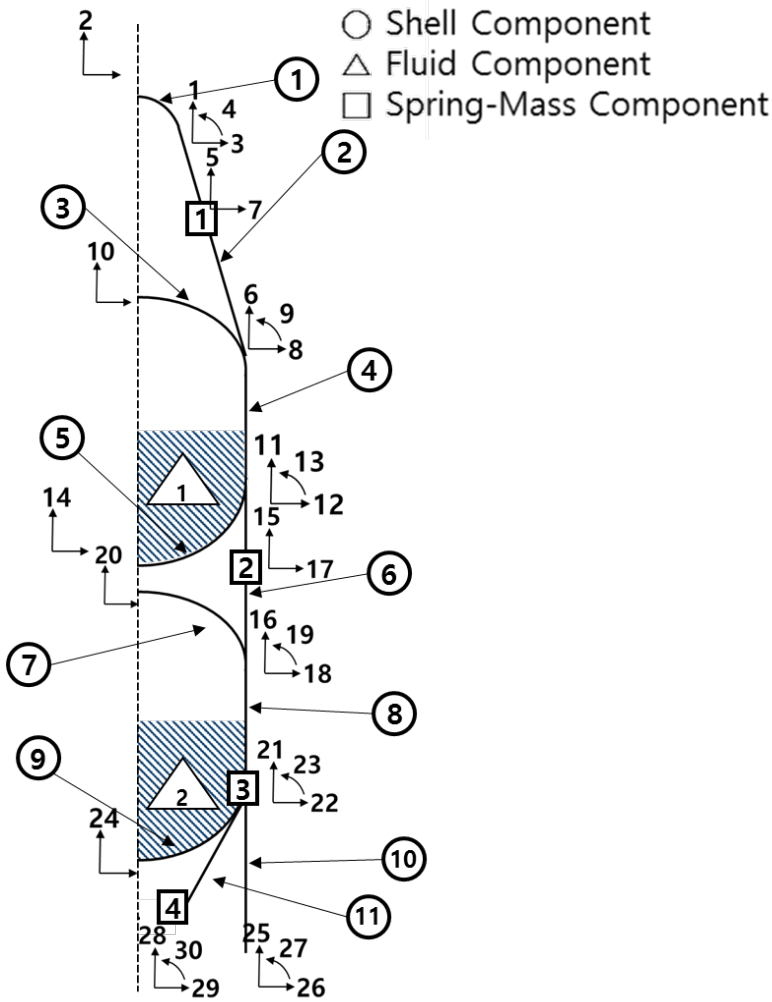

Figure 4.2 Relevant two-dimensional modeling

Table 4.1 Comparison of the natural frequencies between the present prediction and Ref. 41

Mode	Natural frequencies by the present prediction	Natural frequencies in Ref. 41.	Difference (%)
1st mode	37.60	37.67	-0.18
2nd mode	59.94	60.00	-0.10
3rd mode	82.79	83.11	-0.38
4th mode	114.80	114.81	-0.01
5th mode	177.22	177.22	0.00

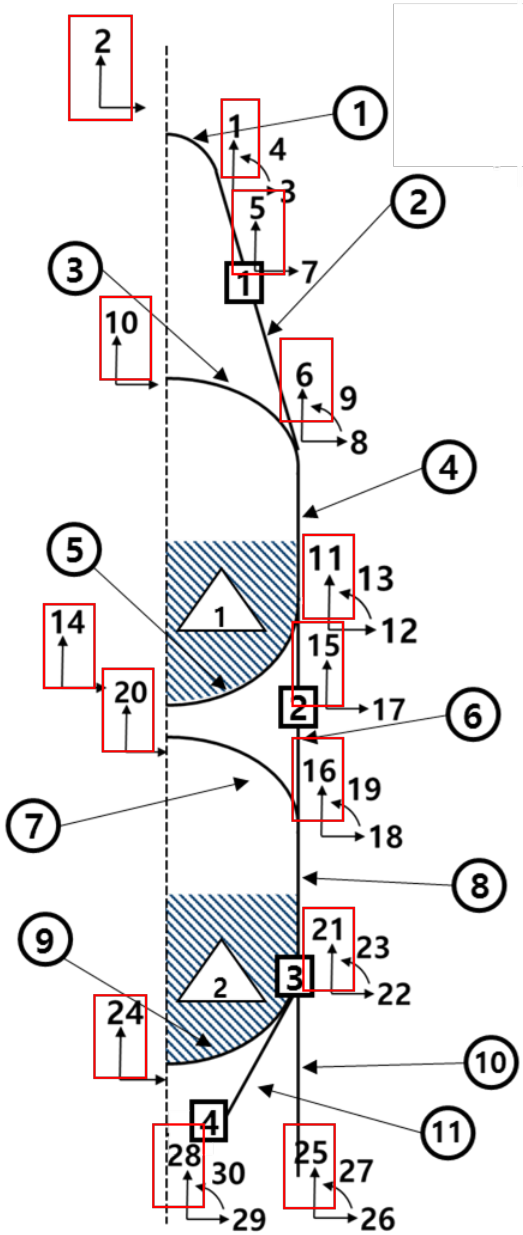

Figure 4.3 Numbering of the longitudinal direction coordinates in relevant two-dimensional modeling

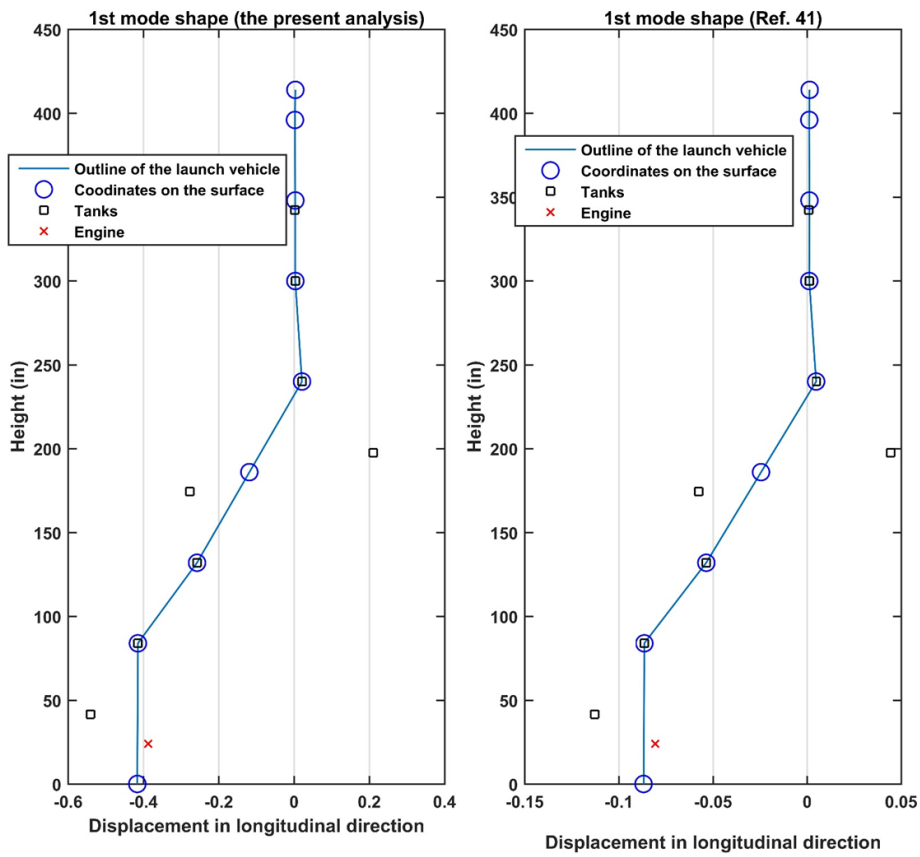

(a) Present prediction **(b) mode shapes in Ref. 41**

Figure 4.4 Comparison of the 1st mode shape

between the present prediction and those in Ref. 41

Table 4.2 Natural frequencies of example single-stage launch vehicle in the present analysis

Mode	Natural frequencies (Hz)
1st mode	37.60
2nd mode	59.94
3rd mode	82.79
4th mode	114.80
5th mode	177.22
6th mode	224.79
7th mode	289.89
8th mode	376.16
9th mode	450.34
10th mode	469.97
11th mode	475.33
12th mode	512.31
13th mode	539.82
14th mode	546.67
15th mode	552.68
16th mode	692.26
17th mode	738.07
18th mode	790.52
19th mode	838.53
20th mode	864.86
21st mode	915.48
22nd mode	949.95
23rd mode	1079.05
24th mode	1367.32
25th mode	1528.78
26th mode	1659.36
27th mode	1718.00
28th mode	1968.86
29th mode	3753.43

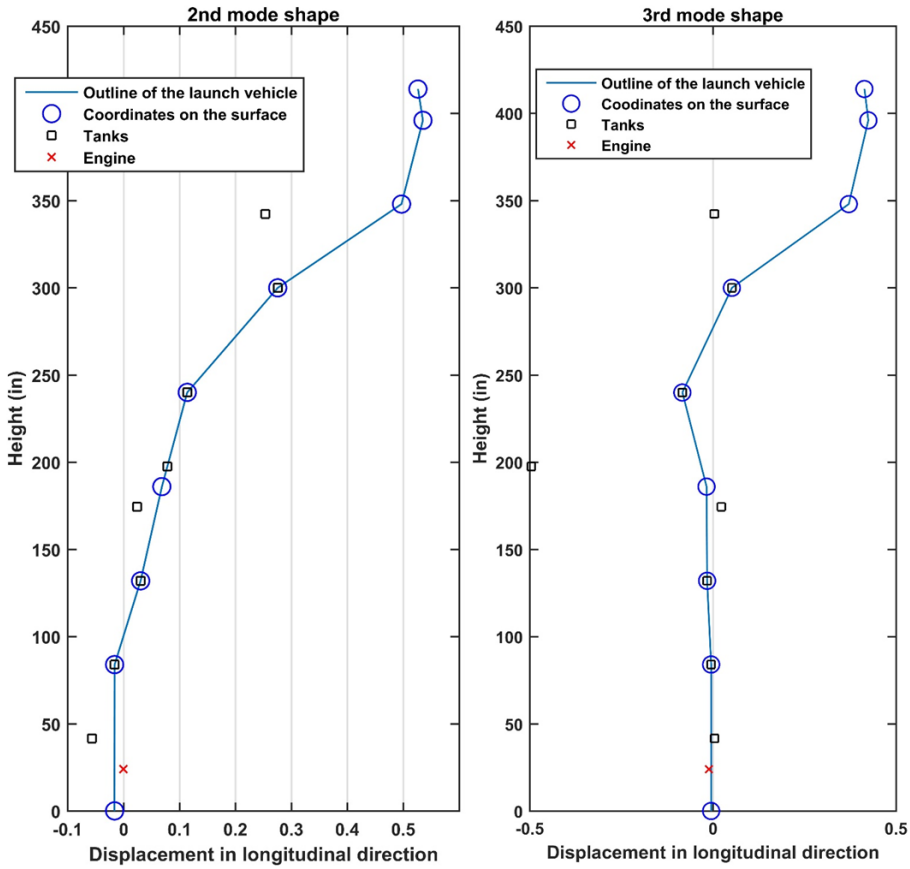

(a) 2nd mode shape **(b) 3rd mode shape**

Figure 4.5 2nd and 3rd mode shapes by the present analysis

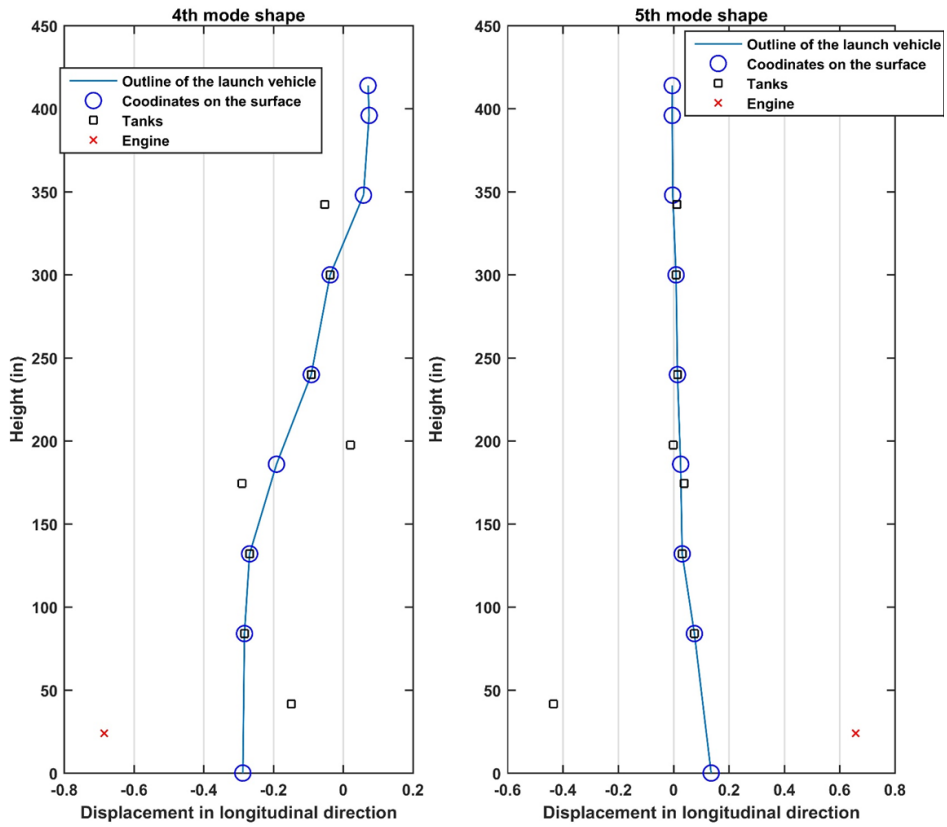

(a) 4th mode shape **(b) 5th mode shape**

Figure 4.6 4th and 5th mode shapes by the present analysis

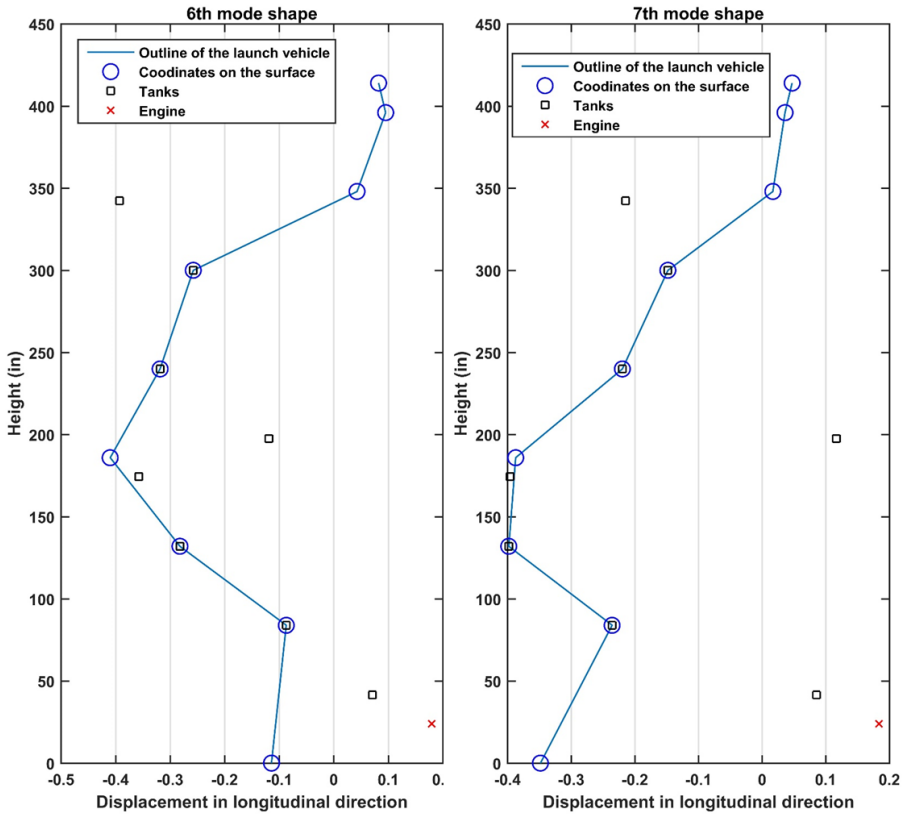

(a) 6th mode shape **(b) 7th mode shape**

Figure 4.7 6th and 7th mode shapes by the present analysis

Chapter 5

Conclusion and Future Works

5.1 Conclusion

This thesis develops the foundation and the method for the research about the pogo phenomenon by examining and referring to the previous researches. Those articles dealt with various launch vehicles in Europe and Asia as well as the famous launch vehicles of U.S.: Delta, Atlas, Titan, Saturn V, and space shuttle.

Accurate prediction capability is required for the pogo phenomenon in a liquid launch vehicle. This thesis is especially focused on the structural modeling and modal analysis of a liquid launch vehicle. More specifically, the transfer function *G(s)* is to be estimated for developing the pogo system. Formulation and the analysis program are developed using the idea of the axisymmetric shell element. The present in-house program is validated by comparing with the existing analytical predictions.

The present methodology using the axisymmetric shell element adopts Rayleigh-Ritz method. In this methodology, a liquid launch vehicle is divided into the following three components; spring-mass, shell, and fluid components. The present shell element is different from that used in the general finite element method. Furthermore, fluid component does not generate additional degree of

freedom.

The present in-house program is developed using the methodology mentioned above. Differences in the mass and stiffness matrix compared with the existing analytical predictions are smaller than 2%. In more detail, the present numerical integration was conducted using a variable size of steps for more accuracy instead of 16-point Gaussian weighting methodology. As a result, prediction of the natural frequencies and mode shapes using the present in-house program is in good agreement. This suggests that present in-house program will be accurate enough for structural modeling and modal analysis of the other launch vehicles.

5.2 Future Works

In the future, the other launch vehicles will be analyzed by using the present methodology. Finally, these results will be used to create the pogo system. The chances of the natural frequencies to overlap with those of the feedlines and propulsion system will be estimated.

This thesis is focused on only the modal analysis of complete launch vehicle without specific information of feedlines, pumps, and engines. But, the mode shapes of the propulsion system will be required in case of the space shuttle. More computation will be needed for understanding and estimation of those mode shapes.

References

[1]Ryan, S. G., “Vibration Challenges in the Design of NASA's Ares Launch Vehicles,” 2009 International Design Engineering Technical Conference: 22nd Biennial Conference on Mechanical Vibration and Noise, 30 Aug. - 2 Sep. 2009, San Diego, US.

[2]Larsen, C. E., “NASA Experience with Pogo in Human Spaceflight Vehicles,” NATO RTO Symposium ATV-152 on Limit-Cycle Oscillations and Other Amplitude-Limited, Self-Excited Vibrations, May 5-8, 2008, Norway.

[3]Rubin, S., “Prevention of Coupled Structure-Propulsion Instability (POGO) on the Space Shuttle,” Space Transportation System-Technology Symposium II – Dynamics and Aeroelasticity, July 15-17, 1970, Cleveland, US.

[4]Fenwick, J., “POGO. Threshold: Pratt & Whitney Rocketdyne’s Engineering Journal of Power Technology,” 1992.

[5]Rubin, S., “Longitudinal Instability of Liquid Rockets Due to Propulsion Feedback (POGO), J. Spacecraft, Vol. 3, No. 8, 1966, pp. 1188-1195.

[6]Oppenheim, B.W., and Rubin, S., “Advanced Pogo Stability Analysis for Liquid Rockets,” Journal of Spacecraft and Rockets, Vol. 30, No.3, 1993, pp. 360-373.

[7]Payne, J., G., and Rubin, S., “Pogo Suppression on the Delta vehicle,” AD-784833, 1974.

[8]McKenna, K., J., Walker, J., H., and Winje, R., A., “A Model for Studying the Coupled Engine-Airframe Longitudinal Instability of Liquid Rocket Systems,” AIAA Aerospace Sciences Meeting, Jan 20-22, 1964, New York, US.

[9]Norquist, L., Marcus, J., and Ruscio, D. “Development of close-coupled accumulators for suppressing missile longitudinal oscillations (POGO),” 5th Propulsion Joint Specialist Conference, June 9-13, 1969, Colorado Springs, USA.

[10]Worlound, A., L., Hill, R., D., and Murphy, G., L., “Saturn V Longitudinal Oscillation (POGO) Solution,” AIAA 5th Propulsion Joint Specialist Conference, June 9-13, 1969, Colorado, USA.

[11]von Pragenau, G., L., “Stability Analysis of Apollo-Saturn V Propulsion and Structure Feedback Loop,” AIAA Guidance, Control, and Flight Mechanics Conference, Aug 18-20, 1969, New Jersey, USA.

[12]Ryan, R., S., Papadopoulos, J., G., Kiefling, L., A., Odum, R., Jarvinen, W., and Kennoy, J., “A Study of Saturn AS-502 Coupling Longitudinal Structural Vibration and Lateral Bending Response during Boost,” AIAA 7th Aerospace Sciences Meeting, Jan 20-22, 1969, New York, USA.

[13]Ryan, R., S., Kiefling, L., A., and Buchanan, H., J., “Simulation of Saturn V S-II Stage Propellant Feedline Dynamics,” *Journal of Spacecraft*, Vol. 7, No. 12, 1970.

[14]Doiron, H., H., “Space Shuttle Pogo Prevention,” Society of Automotive Engineers Aerospace Meeting, Nov 14-17, 1977, Los Angeles, USA.

[15]Rubin, S., Wagner, R., G., and Payne, J. G., “Pogo Suppression on Space Shuttle Early Studies,“ NASA CR-2210, 1973.

[16]Lock, M., H., and Rubin, S., “Passive Suppression of Pogo on the Space Shuttle,“ NASA CR-132452, 1974.

[17]Lock, M., H. and Rubin, S., “Active Suppression of Pogo on the Space Shuttle,“ NASA CR-134749, 1974.

[18]Seidel, R., C., Lorenzo, C., F., and Lehtinen, B., “Space Shuttle POGO Active Controller Design using Frequency Domain Optimization,” NASA TM X-3368, 1976.

[19]Lehtinen, B. and Lorenzo, C., F., “Space Shuttle Active-Pogo-Suppressor Control Design Using Linear Quadratic Regulator Techniques,” NASA Technical Paper 1217, 1979.

[20]Lock, M., H. and Rubin, S., “Analysis of POGO on the Space Shuttle Accumulator Design Guidelines and Planar Multiengine Model Development,” NASA CR-15113, 1976.

[21]Swanson, L., and Giel, T., “Design Analysis of the Ares I Pogo Accumulator,” 45th AIAA/ASME/SAE/ASEE Joint Propulsion Conference & Exhibit, Aug 2-5, Denver, USA.

[22]Anonymous, NASA Space Vehicle Design Criteria-Prevention of Coupled Structure-Propulsion Instability (POGO), NASA SP-8055, 1970.

[23]About, G., Hauguel, P., and Hrisafovicck, N., “La prévention des instabilités pogo sur ariane 1,” *Acta Astronautia*, Volume 10, Issue 4, April 1983, Pages 179-188, in French.

[24]About, G., Bouveret, P., and Bonnal, C., “A New Approach of Pogo Phenomenon Three-dimensional Studies on the Ariane 4 Launcher,” *Acta Astronautia*, Volume 15, Issues 6–7, June–July 1987, Pages 321-330.

[25]Dordain, J., J., Lourme, D., and Estoueig, C., “Etude de l'effet POGO sur les lanceurs EUROPA II et DIAMANT B,” *Acta Astronautia*, Volume 1, Issues 11–12, November–December 1974, Pages 1357-1384, in French.

[26]Ono Y., Kohsetsu Y., and Shibukawa, K., “POGO Ground Simulation Test of H-I Launch Vehicle's Second Stage,” 28th Structures, Structural Dynamics and Materials Conference, Structures, Structural Dynamics, and Materials Conferences, April 6-8, 1987, Monterey, USA.

[27]Ujino, T., Morino, Y., Kohsetsu, Y., Mori, T., and Shirai, Y., “POGO Analysis on the H-II Launch Vehicle,” 30th Structures, Structural Dynamics and Materials Conference, April 3-5, 1989, Mobile, USA.

[28]Ujino, T., Shimura, T., Kohsetsu, Y., and Niitsu, M., “POGO Prevention of H-2 Launch Vehicle", 35th Structures, Structural Dynamics, and Materials Conference, aterials Conference, April 18-20, 1994, USA.

[29]Zhao, Z., and Ren, G., “Parameter Sturdy on Pogo Stability of Liquid Rockets,” *Journal of Spacecraft and Rockets*, Vol. 48, No. 3, 2011.

[30]Xu, D., Hao, Y., and Tang, G., “New Pogo Analysis Method Using Rational Fitting and Three-Dimensional Tank Modeling,” *AIAA Journal*, Nol. 53, No. 2, 2015.

[31]Hao, Y., Tang, G., and Xu, D., “Finite-Element Modeling and Frequency-Domain Analysis of Liquid-Propulsion Launch Vehicle,” *AIAA Journal*, Nol. 53, No. 11, 2015.

[32]Lee, H., J., Jung, T., K., Menshikova, O., M., Kim, Y., W., Cho, I., H., Oh, S., H., and Lee, D., S., “Pogo Analysis on the KSR-Ⅲ Propulsion Feeding System,” *Journal of the Korean Society of Propulsion Engineers*, Vol. 6 No. 3, 2002.

[33]Chang, H., S., “A Study on the Analysis of Pogo and its Suppression,” Master’s Thesis, KAIST, 2002.

[34]Alley, V., L., and Gerringer, A., H., “A Matrix Method for the determination of the Natural Vibrations of Free-Free Unsymmetrical Beams with Application to Launch Vehicles.” NASA TN D-1247, 1962.

[35]Wingate, R., T., “Matrix Analysis of Longitudinal and Torsional Vibrations in Nonuniform Multibranch Beams,” NASA TN D-3844, 1967.

[36]Pinson, L., D., “Longitudinal Spring Constants for liquid-Propellant Tanks with Ellipsoidal Ends,” NASA TN D-2220, 1964.

[37]Kana, D., D., and Gormley, J., F., “Longitudinal Vibration of a Model Space Vehicle Propellant Tank,” J. Spacecraft, Vol. 4, No. 2, 1967, pp. 1585-1591.

[38]Pengelley, C., D., "Natural Frequency of Longitudinal Modes of Liquid Propellant Space Launch Vehicles," J. Spacecraft, Vol. 5, No. 12, 1968, pp. 1425-1431.

[39]Anonymous, NASA Space Vehicle Design Criteria-Natural Vibration Modal Analysis, NASA SP-8012, 1970.

[40]Anonymous, NASA Space Vehicle Design Criteria-Structural Vibration Prediction, NASA SP-8050, 1970.

[41]Archer, J., S., and Rubin, C., P., "Improved Analytic Longitudinal Response Analysis for Axisymmetric Launch Vehicle," Volume 1, NASA CR-345, 1965.

[42]Rubin, C., P., and Wang., T., T., "Improved Analytic Longitudinal Response Analysis for Axisymmetric Launch Vehicle," Volume 2, NASA CR-346, 1965.

[43]Lawler, W., H., and Riley, G., F., "Saturn V Structural Dynamic Test/Modeling," 41st AIAA/ASME/ASCE/AHS/ASC Structures, Structural Dynamics, and Materials Conference and Exhibit, April 3-6, 2000, Atlanta, USA.

[44]Pinson, L., D., and Leadbetter, S., A., "Some Results from 1/8-Scale Shuttle Model Vibration Studies," *Journal of Spacecraft*, Vol. 61, No. 1, 1979.

[45]Kim, J., "Structural Modeling and Dynamic Analysis Reflecting Liquid Propellant for Longitudinal Dynamic Instability (POGO) of Aerospace Vehicle," Master's Thesis, Seoul National University, 2016.

[46]Kim, J., Sim, J., Shin, S., Park, J., and Kim, Y., "Advanced One-dimensional Dynamic Analysis Methodology for Space Launch Vehicles Reflecting Liquid Components," *Aeronautical Journal*, preparing 1st revision.

[47]Gerus, T., Housely, F., J., A., and Kusic, G., “Atlas-Centaur-Surveyor Longitudinal Dynamics Tests,” NASA TM X-1459, 1967.

[48]Sim, J., Kim, J., Lee, S., Shin, S., Choi, H., and Yoon, W., “Further Extended Structural Modeling and Modal Analysis of liquid Propellant Launch Vehicles for Pogo Analysis,” AIAA SPACE Conference and Exposition, Sept 13-16, 2016 Long Beach, USA.

[49]Steret, J., B., and Riley, G., F., “Saturn V/Apollo Vehicle Pogo Stability Problems and Solutions,” AIAA 7th Annual Meeting and Technological Display, Oct 19-22, 1970, Huston, USA.

국문초록

포고 안정성 해석을 위한
유탄성 효과가 고려된 축대칭 쉘 요소를 이용한
우주 발사체의 구조 동적 해석

심 지 수

기계항공공학부

서울대학교 대학원

액체 추진제 우주 발사체에서 여러 시스템의 연성(coupling)에 의해 발생하는 현상으로 몇 가지가 있다. 그 중에서 대표적인 것 중 하나로 우주 발사체의 축방향 동적 불안정성인 포고 현상으로 구조, 공급계, 추진 시스템의 연성에 의해 발생한다. 60~70 년대의 많은 발사체 개발 과정에서 포고 현상이 발생하여 포고 현상을 예측하고 이를 억제하도록 하는 것은 발사체 개발 과정에서 꼭 필요하다. 포고 현상은 우주 발사체의 구조적인 특징이 근본적인 원인이며 추진제 소모에 따라서 전기체 구조 고유진동수가 증가하게 되고 공급계 및 추진 시스템의 고유진동수와 일치하게 되었을 때 구조적인 반응과 공급계, 추진 시스템이 닫힌계 시스템을 형성하게 된다. 따라서 포고 예측을 위해서는 구조, 공급계, 추진 시스템을 모델링을 필수적으로 수행하여야 하며 닫힌계 시스템을 구성하여 그 시스템의 안정성을 판단하다.

본 논문에서는 포고 현상을 예측하기 위하여 시스템 구성을 위한 구조 반응을 예측하는데 초점을 맞추고 있다. 이를 위하여 우주 발사체의 전기체 구조 모델링 및 모드해석이 필요하며 특히 우주 발사체의 추진제 효과를 반영하는 것이 중요하다. 이전에 1 차원 요소를 이용한 구조 모델링에서 발전하여 축대칭 2 차원 요소를 이용한 구조 모델링에 대하여 연구를 진행하였으며 NASA 문서를 토대로 정식화, In-house 프로그램을 작성하였다. 본 기법의 기본적인 정식화 과정은 Rayleigh-Ritz 방법을 이용하며 우주 발사체 전기체를 질량-스프링, 쉘, 유체 요소로 나누어 모델링이 진행된다. 본 기법을 활용할 수 있도록 예시 1 단 발사체 형상과 구조 모델링 과정이 있으며 입력과 결과 값이 있다. 이를 토대로 In-house 프로그램을 작성하였으며 검증을 진행하였다.

또한 Saturn V 와 우주왕복선의 연구 사례를 통하여 전기체 우주 발사체의 모드 해석한 결과를 이용하여 포고 현상의 닫힌계 시스템을 구성하는 방법과 해석 방법에 대하여 연구하였다.

주요어 : 우주 발사체, 포고 현상, 유탄성 효과, 안정성 해석,
구조 모델링, 동적 해석

학 번 : 2015-20778